

## Discovery of New Inhibitors of *Schistosoma mansoni* PNP by Pharmacophore-Based Virtual Screening

Matheus P. Postigo,<sup>†</sup> Rafael V. C. Guido,<sup>†</sup> Glaucius Oliva,<sup>†</sup> Marcelo S. Castilho,<sup>‡</sup> Ivan da R. Pitta,<sup>§</sup> Julianna F. C. de Albuquerque,<sup>§</sup> and Adriano D. Andricopulo<sup>\*,†</sup>

Laboratório de Química Medicinal e Computacional, Instituto de Física de São Carlos, Universidade de São Paulo, Av. Trabalhador São-Carlense 400, 13560-970, São Carlos-SP, Brazil, Faculdade de Farmácia, Universidade Federal da Bahia, R. Barão de Jeremoabo, s/n, 40170-115, Salvador-BA, Brazil, and Departamento de Antibióticos, Universidade Federal de Pernambuco, 50670-901, Recife-PE, Brazil

Received April 4, 2010

Schistosomiasis is considered the second most important tropical parasitic disease, with severe socioeconomic consequences for millions of people worldwide. *Schistosoma mansoni*, one of the causative agents of human schistosomiasis, is unable to synthesize purine nucleotides de novo, which makes the enzymes of the purine salvage pathway important targets for antischistosomal drug development. In the present work, we describe the development of a pharmacophore model for ligands of *S. mansoni* purine nucleoside phosphorylase (*SmpNP*) as well as a pharmacophore-based virtual screening approach, which resulted in the identification of three thioxothiazolidinones (**1–3**) with substantial in vitro inhibitory activity against *SmpNP*. Synthesis, biochemical evaluation, and structure–activity relationship investigations led to the successful development of a small set of thioxothiazolidinone derivatives harboring a novel chemical scaffold as new competitive inhibitors of *SmpNP* at the low-micromolar range. Seven compounds were identified with IC<sub>50</sub> values below 100  $\mu$ M. The most potent inhibitors **7**, **10**, and **17** with IC<sub>50</sub> of 2, 18, and 38  $\mu$ M, respectively, could represent new potential lead compounds for further development of the therapy of schistosomiasis.

### INTRODUCTION

Neglected tropical diseases are the foremost threat to human health and welfare around the world. Schistosomiasis, a major cause of illness, long-term disability, and death, is caused by several species of trematode parasite of the genus *Schistosoma*. The disease is endemic in tropical regions, affecting more than 200 million people spread over about 80 developing countries.<sup>1</sup> Approximately 20 million infected people exhibit severe disease manifestations, including chronic hepatic, intestinal fibrosis, and calcification of the urinary tract.<sup>2</sup> Praziquantel is the only effective drug available for the treatment of schistosomiasis.<sup>3,4</sup> Although the treatment is considerably affordable, less than 20% of those in need currently receive the drug.<sup>2,5</sup> Additionally, praziquantel has been in use for more than 20 years, and significant resistance to the chemotherapy has emerged.<sup>6</sup> Therefore, this scenario highlights the urgent need for the development of new drugs for the chemotherapy of schistosomiasis.

Structure-based enzyme inhibitor design approaches play a crucial role in the development of small-molecule drug candidates that act on specific enzymes and have become a pivotal component of drug discovery programs.<sup>7,8</sup> Structural data for several parasite enzymes are currently available, allowing the use of structure-based drug design (SBDD) for lead discovery and optimization.<sup>9</sup> During the past years, there have been remarkable advances in the study of important

targets for the development of new antiparasitic agents.<sup>10–18</sup>

A potential target for new drugs against schistosomiasis is purine nucleoside phosphorylase (PNP) from *Schistosoma mansoni* (*SmpNP*, EC 2.4.2.1), a key enzyme in the purine salvage pathway.<sup>19–22</sup> In the present work, the development of a 3D pharmacophore-based virtual screening approach has led to the identification of three small-molecule thioxothiazolidinones (**1–3**) with in vitro inhibitory activity against *SmpNP*. Subsequent structure–activity relationship (SAR) studies contributed to the development of a set of thioxothiazolidinone derivatives (**4–20**) as competitive inhibitors of *SmpNP* at the low micromolar range. The structure-based approach was proved experimentally to be suitable for the discovery of a novel chemical scaffold for *SmpNP* inhibitor design.

### RESULTS AND DISCUSSION

**Approach.** A 3D structure-based pharmacophore model was used as a query to search a database of structurally diverse compounds. The selected compounds were experimentally evaluated in vitro against the target enzyme (*SmpNP*). The pharmacophore-based virtual screening approach is summarized in Figure 1.

**Target Protein Structure.** The PNP enzyme catalyzes the reversible phosphorolysis of purine (2'-deoxy)ribonucleosides, in the presence of inorganic orthophosphate (Pi) as a second substrate, to give the corresponding purine base and (2'-deoxy)ribose-1-phosphate as products. *SmpNP* is a homotrimer of molecular mass of 93 kDa, whose subunits are related to each other by a noncrystallographic three-fold symmetry (Figure 2). Each subunit consists of an extended

\* Corresponding author. E-mail: aandricop@ifsc.usp.br. Telephone: +55 16 3373-8095.

<sup>†</sup> Universidade de São Paulo.

<sup>‡</sup> Universidade Federal da Bahia.

<sup>§</sup> Universidade Federal de Pernambuco.

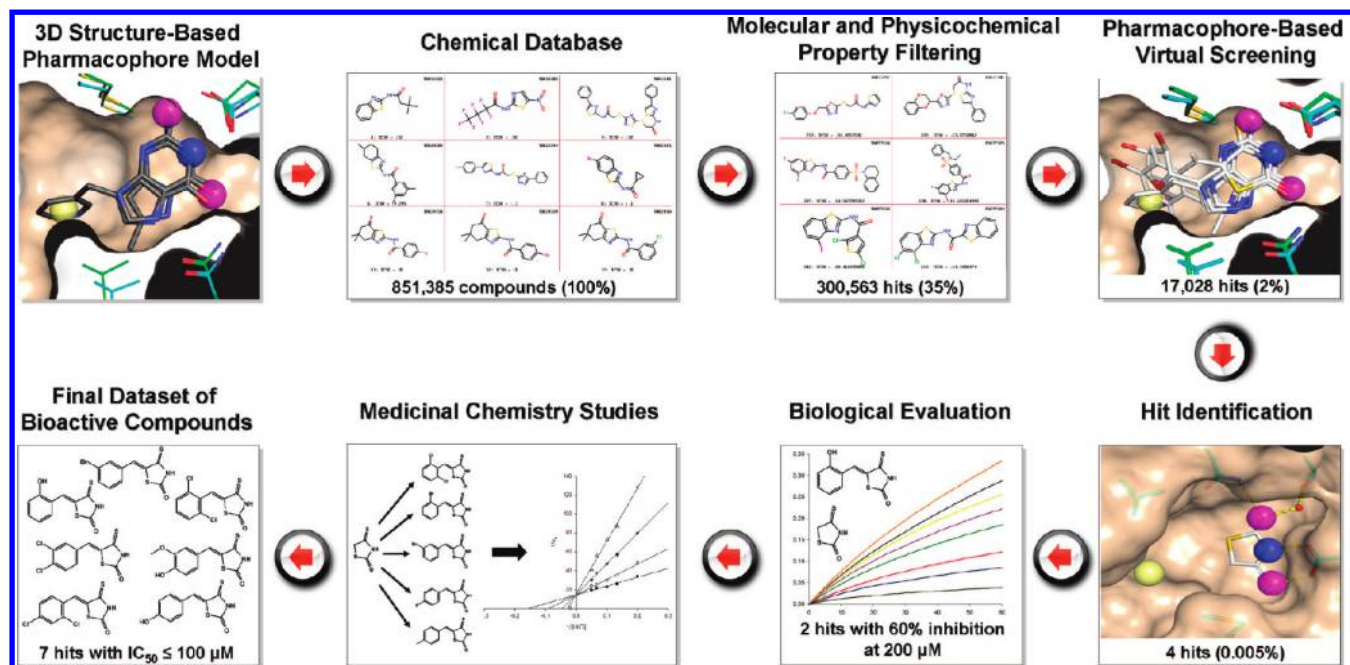


Figure 1. Development of a pharmacophore-based virtual screening approach for *Sm*PNP inhibitors.

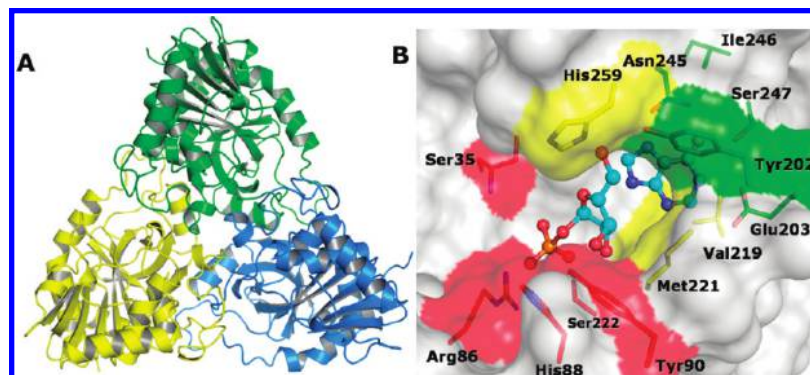


Figure 2. (A) Quaternary structure of *Sm*PNP (PDB ID 3FNQ). (B) Close inspection of the *Sm*PNP active site. The figure shows a schematic model of hypoxanthine and ribose-1-phosphate (ball-and-stick model) as products of the enzymatic reaction catalyzed by PNP. The purine base-, ribose-, and phosphate-binding sites are colored in green, yellow, and red, respectively.

mixed nine stranded  $\beta$ -sheet surrounded by seven  $\alpha$ -helices and four  $3_{10}$ -helices.<sup>23</sup> The active site is divided into three subsites: purine base-, ribose-, and phosphate-binding sites (Figure 2).

Currently, 12 crystal structures of *Sm*PNP in complex with a variety of ligands are deposited in the Protein Data Bank (PDB), as shown in Table 1. In particular, two of these structures (PDB IDs 1TCU and 1TD1)<sup>24</sup> contain ions which were obtained from the crystallization buffers (e.g., acetate, phosphate, and/or sulfate). Three structures correspond to the complex of *Sm*PNP with its natural substrate inosine (PDB ID 3FAZ)<sup>23</sup> and to the products of the enzyme-catalyzed reaction, hypoxanthine and ribose-1-phosphate (PDB IDs 3FNQ and 3FB1, respectively).<sup>23</sup> One of the complexes contains the crystallization nondetergent additive sulfobetaine 195 (PDB ID 1TCV),<sup>24</sup> and the six remaining crystallographic models represent the bound state of the parasite enzyme with the substrate analogs adenine, adenosine, and guanosine (PDB IDs 3E9R, 3F8W, 3IEEX, respectively)<sup>22,23</sup> as well as with the small-molecule inhibitors 6-chloroguanine, 9-deazaguanine, and tetrahydropyrimidine derivatives (PDB IDs 3E9Z, 3DJF, and 3E0Q, respectively). The superposition of the C $\alpha$  atoms of the trimers revealed

that the overall structure topology of the different complexes is quite similar with root-mean-square deviation (rmsd) values  $<0.5$  Å, suggesting that little conformational changes occur upon ligand binding.

In order to provide new insights into the structural requirements for PNP binding affinity, a structural analysis of the active site was also conducted using the homologous bovine enzyme (*Bos taurus*, *Bt*PNP), for which several high-resolution crystallographic structures have been determined (Table 1). Interestingly, while *Bt*PNP shares approximately 50% sequence identity to *Sm*PNP, it can be observed in Figure 3 that the amino acid sequence within the active site region is greater than 90%.<sup>22</sup>

Table 1 shows that some of the *Bt*PNP complexes are similar to those of *Sm*PNP (e.g., 1A9R:3FNQ and 1A9Q:3FNQ), whereas others are only found in *Bt*PNP, as is the case of the complexes with the substrate analogue 9-deazainosine (PDB ID 1A9P);<sup>25</sup> and with the inhibitors *N*(7)-acycloguanosine (PDB ID 1FXU),<sup>26</sup> 9-(5,5-difluoro-5-phosphonopentyl)guanine (PDB ID 1V48),<sup>27</sup> and 4-amino-7-methylpyrazolo[1,5-a][1,3,5]triazin-2(1H)-one (PDB ID 2QLP).<sup>28</sup> The structural comparison of the *Bt*PNP ligand-protein complexes revealed that the overall topology is

**Table 1.** Crystallographic Structures of *S. mansoni* and Bovine PNPs Employed for the 3D Pharmacophore Model Generation

Organism	PDB ID	Resolution (Å)	Ligand I	Ligand II
<i>S. mansoni</i>				
	1TCU	2.00		
	1TD1	1.90		---
	3FAZ	1.90		
	3FNQ	1.85		
	3FB1	2.00		
	1TCV	1.75		
	3E9R	1.85		
	3F8W	2.30		
	3IEX	2.05		---
	3E9Z	2.31		
	3DJF	2.30		---
	3E0Q	1.90		---

Table 1. Continued

Organism	PDB ID	Resolution (Å)	Ligand I	Ligand II
<i>Bovine</i>				
	1A9O	2.00		---
	1A9P	2.40		
	1A9Q	2.00		
	1A9R	2.00		
	1A9S	2.00		---
	1A9T	2.00		
	1FXU	2.20		---
	1V48	2.20		---
	2QPL	2.10		---
	3PNP	1.60	Mg <sup>2+</sup>	
	4PNP	1.80		---



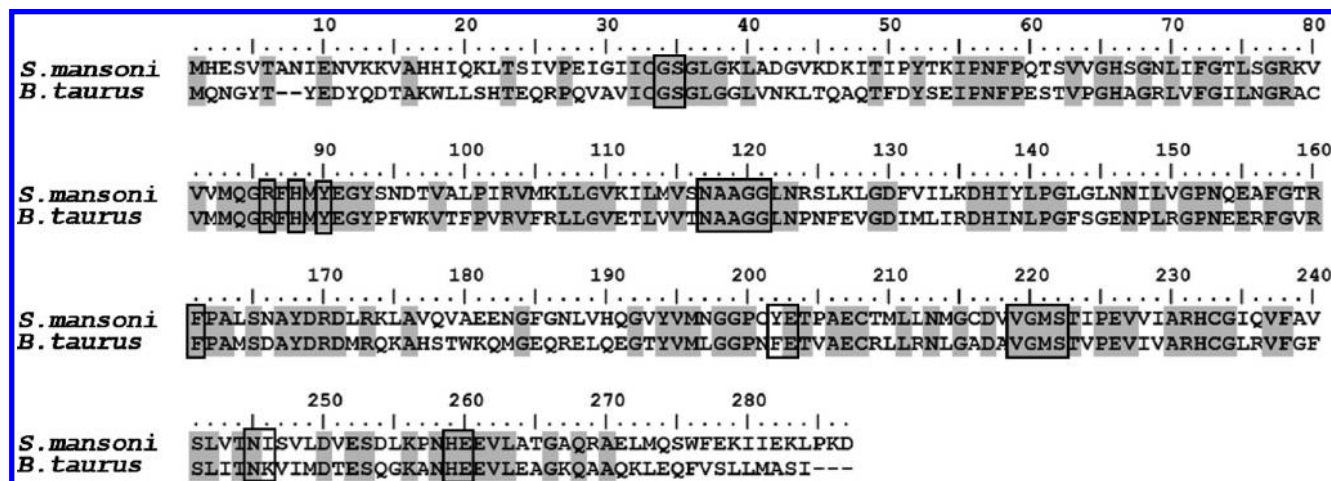


**Figure 3.** Sequence alignment of *Sm*PNP and *Bt*PNP (first and second lane, respectively). Pairwise alignment with BLOSUM62 matrix shows that *Sm*PNP:*Bt*PNP share 48% sequence identity. The numbers above the sequences refer to the *Sm*PNP sequence. Conserved residues are highlighted in gray, and active site residues are boxed. The alignment was carried out with the CLUSTALW program.

similar in all cases (rmsd values  $<0.30$  Å), and only local conformational changes (e.g., side-chain shifts) are necessary to accommodate the ligands within the binding cavity.

**Pharmacophore Model Generation.** The molecular binding process relies on several properties and features of the amino acids present in the active site.<sup>29</sup> According to the IUPAC definition, a pharmacophore is the ensemble of steric and electronic features that is necessary to ensure the optimal supramolecular interactions with a specific biological target structure and to trigger (or to block) its biological response.<sup>30</sup> The aim of the present study is to design a robust three-dimensional (3D) pharmacophore-based virtual screening approach in order to identify new structural scaffolds for the development of competitive inhibitors of *Sm*PNP. In this way, a detailed structural study was conducted for the 23 PNP structures of Table 1 to generate a receptor-based pharmacophore model. Accordingly, the crystal structures of *Sm* and *Bt* PNPs were superimposed on each other, with respect to the backbone C $\alpha$  atom, to investigate the structural requirements for optimal competitive inhibition of *Sm*PNP (Figure 4A). Although several water molecules are displaced from the binding site, a crystallographic water molecule is found in all examined *Sm*PNP crystal structures at equivalent positions (base-binding site, Figure 4B). The water molecule assists the stabilization of the ligand–protein complexes through a hydrogen-bonding network, involving the 6-oxo group of the purine base and the side chain of the Ser247 residue. The sequence comparison of Figure 3 revealed that Ser247 in *Sm*PNP is replaced with Val245 in *Bt*PNP. This mutation would affect the hydrogen-bonding interactions of the specific subsite, providing new opportunities for the design of selective *Sm*PNP inhibitors.<sup>22</sup>

The purine-binding subsite is rather rigid, with only Asn245 (Asn243 in *Bt*PNP) exhibiting alternative conformations upon ligand binding (Figure 4B). This residue lies close to the crystallographic water molecule, and a structural analysis of the complexes showed that a flip of the side chain of Asn245 may occur depending on the characteristics of the ligand molecule. The flip in the orientation of the carbonyl or amino groups toward the active site is related to the physicochemical properties of the ligand. In light of this, the first pharmacophore point was assigned to the region

favorable for hydrogen-bond donor/acceptor interactions (Figure 4C).

The structural comparison of the PNP complexes underscores the mode of interaction of several ligands. The rigid moiety of the ligands (e.g., purine base) was used as a reference to identify the physicochemical properties directly related to protein–ligand binding affinity. Interestingly, the analysis suggests that putative ligands should exhibit both hydrogen-bond donor and acceptor features to interact with the conserved residue Glu203 (Glu201 in *Bt*PNP, Figure 4B). These interactions are presumably facilitated by the low pH in which the *Sm*PNP complexes were crystallized.<sup>24,28</sup> The typical  $pK_a$  value of the carboxyl group of glutamic acid residues is about 5, which is close to the pH of the *Sm*PNP crystallization experiments (pH 4.9–5.0). In addition, a close inspection of the crystal structures indicated that the symmetry and distance of the hydrogen-bond interactions between ligands and Glu203 correspond to the protonated side chain. Hence, two pharmacophore points were assigned to the favorable regions for hydrogen bond near to the side chain of Glu203 (Figure 4C). The information gathered from the different binding mode of the ligands allowed the identification of a favorable region for hydrophobic interactions, incorporating the side chains of Met221 and Val262 (Met219 and Val260 in *Bt*PNP, respectively). Thus, the fourth pharmacophore point was defined as the most favorable area for hydrophobic interactions.

The final four-point pharmacophore model (Figure 4C) consists of: (i) a hydrogen donor/acceptor point close to Asn245 and the crystallographic water; (ii) a second hydrogen donor/acceptor point in the proximity of the protonated hydroxyl group of Glu203; (iii) one hydrogen donor point close to the C=O group of Glu203; and (iv) a pharmacophore point defined to incorporate the most favorable area for hydrophobic interactions with the residues Met221 and Val262 of the protein cavity.

**Database for Virtual Screening.** A database of 851 385 commercially available compounds was selected from the ZINC database.<sup>30</sup> These compounds were selected from the following chemical databases: ChemBridge (443 783 compounds), Asinex (307 468 compounds), and Ambinter (100 134 compounds). Several molecular filters were applied in order

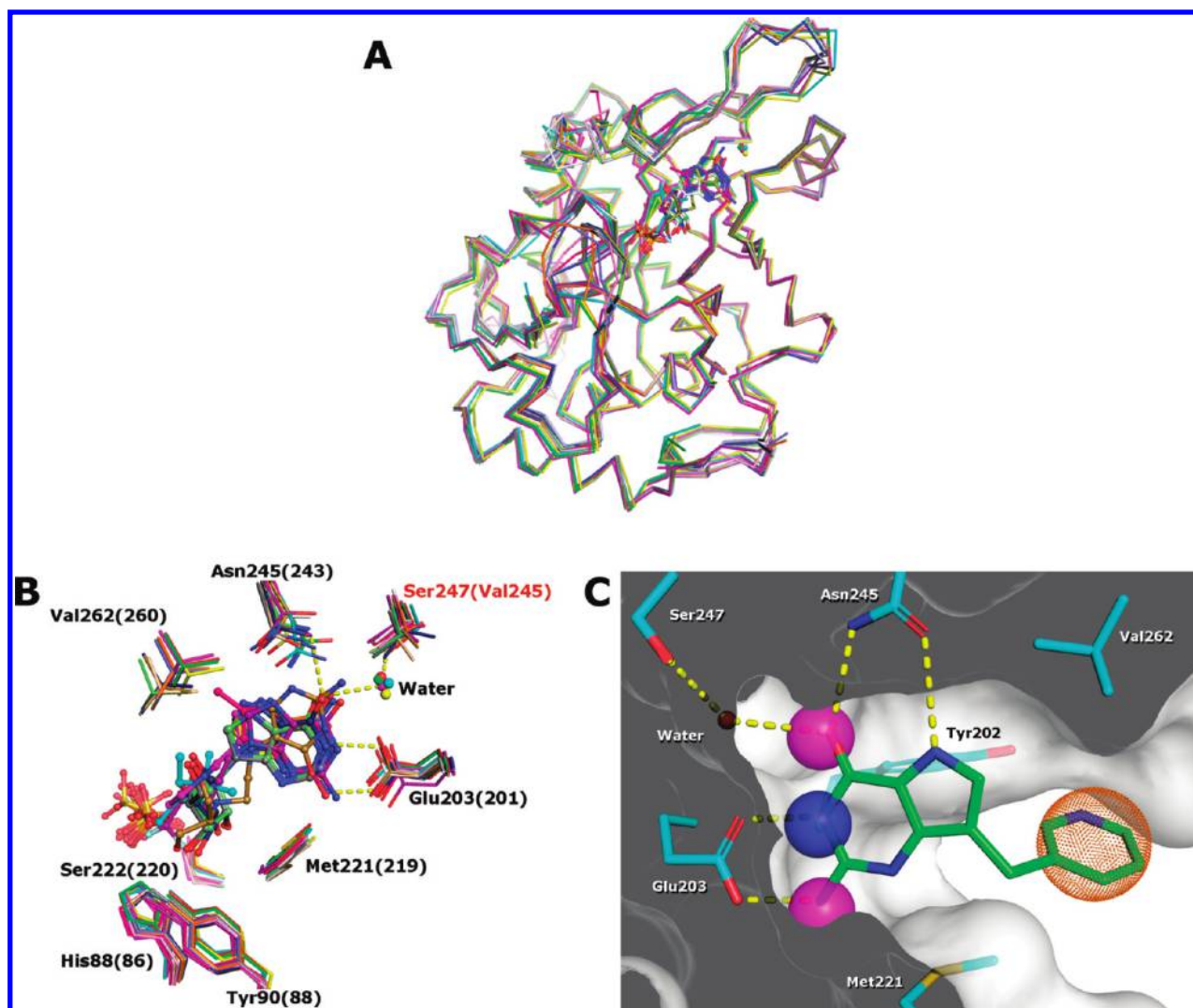


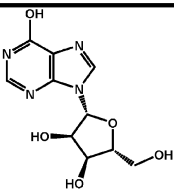
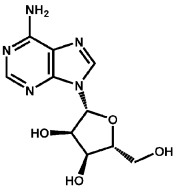
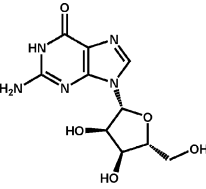
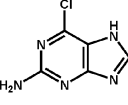
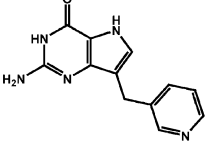
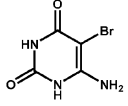
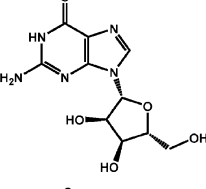
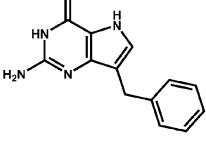
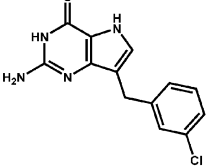
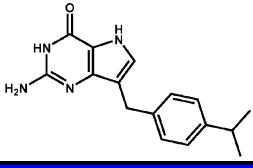
**Figure 4.** (A) Structural superposition of the 23 PNP crystal complexes (Table 1) used to derive the structure-based pharmacophore model. (B) Close-up view of the catalytic amino acid residues and key hydrogen bonds involved in ligand recognition. The catalytic residues from both *Sm*PNP and *Bt*PNP are depicted as stick models, whereas the ligands are represented as ball-and-stick models and the *Sm*PNP crystallographic water as spheres. Hydrogen bonds are drawn as dashed lines. Nonconserved and conserved residues between species are indicated in red and black (*Bt*PNP residues numbers are shown in parentheses). (C) The four-point pharmacophore-based model employed for virtual screening. The hydrophobic interaction (orange-dotted sphere) to the side chains of Val262, Met221, and Tyr202 was considered in the virtual screening process. The donor and acceptor features are depicted in blue and magenta, respectively. The ligand BCX-34 (PDB ID 3DJF) is shown in green, and the binding site residues are in cyan.

to reduce the number of compounds in the database. Initially, all molecules containing an atom other than H, C, N, O, S, P, F, Cl, Br, or I were removed. The molecules retrieved from the chemical database were further evaluated using pharmacokinetic property filters based on the Lipinski's rule of five.<sup>31</sup> Accordingly, molecules with molecular weight greater than 500, calculated  $\log P$  greater than 5, and more than 5 hydrogen-bond donors, or 10 hydrogen-bond acceptors were also removed from the chemical database. Only a filtered subset of 300 563 compounds was used in the virtual screening experiments. A set of 10 characterized *Sm*PNP ligands was included in the 3D pharmacophore database search. In the early steps of our search, the appearance of these compounds in the list of prospective hits served to calibrate and control our 3D search method. The members of the test set are listed in Table 2. Among them, six ligands were considered whose binding mode was determined crystallographically. Other four potent inhibitors ( $IC_{50}$  values ranging from 0.5 to 95  $\mu M$ ) were included to increase the

structural diversity of the reference set. The molecular weight of the test set inhibitors lies between 169 and 299 Da, and the calculated  $\log P$  is between  $-3.66$  and  $2.90$ .

**Structure-Based Virtual Screening.** The 3D pharmacophore model was translated into a flexible search query appropriate for the 3D search with UNITY,<sup>32</sup> highlighting the spatial arrangement of chemical features that represents the essential interactions of small-molecule ligands and *Sm*PNP. The four search tolerance spheres were placed by picking the appropriate atoms of the ligand BCX-34 bound to the PNP active site (PDB ID 3DJF), and their diameters were manually adapted in order to cover the favorable areas indicated by the structural analysis. A database containing 300 563 molecules was screened, and three out of the four-point pharmacophores were required in the 3D searches. According to these criteria, the 10 test set ligands were successfully retrieved from the database. A subset of 17 028 compounds that matched the pharmacophore was selected. Out of these, 457 could be oriented to establish hydrogen

**Table 2.** Test Set Compounds Used to Calibrate and Control the 3D Pharmacophore Search

Compound	PDB	Biological Property	cLog <i>P</i> *	MM (Da)	Reference
	3FAZ	$K_M = 7 \mu\text{M}$	-1.52	268	22
	3F8W	$IC_{50} = 83 \mu\text{M}$	-2.15	267	23
	3IEX	---	-3.14	283	22
	3E9Z	---	0.58	169	---
	3DJF	$IC_{50} = 0.8 \mu\text{M}$	-0.03	241	22
	3E0Q	---	-0.50	206	---
	---	$IC_{50} = 95 \mu\text{M}$	-3.66	299	22
	---	$IC_{50} = 1.4 \mu\text{M}$	1.47	240	22
	---	$IC_{50} = 0.5 \mu\text{M}$	2.18	274	22
	---	$IC_{50} = 0.15 \mu\text{M}$	2.90	282	22

\* Calculated log *P*: property computed by the ClogP program implemented in SYBYL8.0.



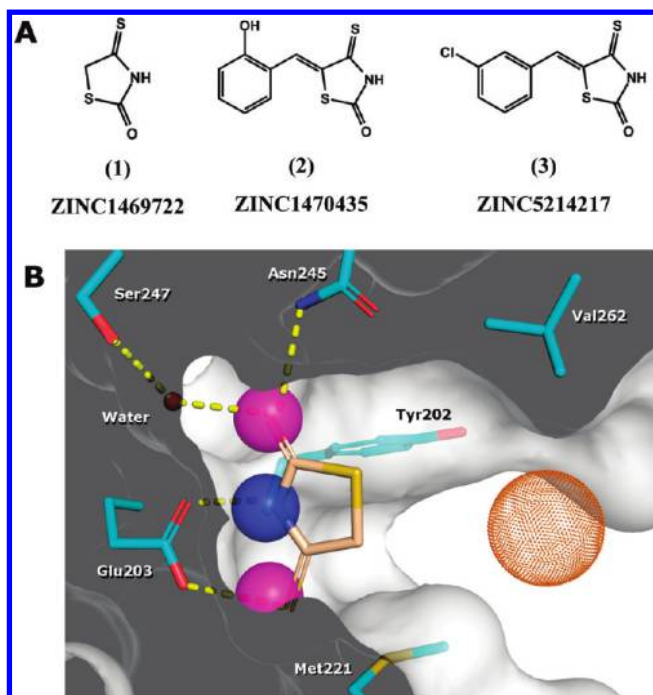


**Figure 5.** (A) Hits from the virtual screening approach. (B) Selected hit (ZINC1469722) that satisfies the pharmacophore requirements and the hydrogen-bonding network (color code described in Figure 4C). Hydrogen bonds are depicted as yellow dashed lines.

bonds to the side chains of Asn245 and Glu203, as found in the high-resolution structure of *SmpNP* in complex with substrate analogs (PDB IDs 3E9R, 3F8W, and 3IEX) and small molecules inhibitors (PDB IDs 3E9Z, 3DJF, and 3E0Q). These molecules possess substantial chemical diversity, including a variety of guanine, cytosine, and thymine derivatives as well as a number of tetrazoles, thiazolidines, and thioxothiazolidinones. The 100 top-ranked molecules from each chemical class were docked into the *SmpNP* active site using FlexX.<sup>33</sup> The crystallographic water molecule was considered in the protein binding pocket during the docking simulations.

The predicted binding modes in the *SmpNP* binding site were ranked based on their relative affinity using the scoring functions implemented in FlexX and DrugScore.<sup>34</sup> Visual inspections of the predicted binding modes along with the scoring values provided by FlexX and DrugScore were used to select the final set of compounds. The criteria used in the visual inspection for the assessment of the compounds included: (i) structural novelty and innovative scaffold for the design of *SmpNP* inhibitors; (ii) overall matching of the hydrogen-bonding network, with emphasis on the formation of hydrogen bonds to Asn245 and to the crystallographic water; (iii) complementarity between ligands and protein surfaces in terms of spatial occupancy; and (iv) structures with less than three rotatable bonds to avoid entropically unfavorable binding. The final subset of compounds consisted of three thioxothiazolidinones that were selected and evaluated against *SmpNP* (Figure 5).

**Biochemical Evaluation and SAR Studies.** The compounds **1–3** showed in vitro inhibitory activity against *SmpNP*, with about 50–90% inhibition at a single concentration of 200  $\mu\text{M}$ . Subsequently, values of  $\text{IC}_{50}$  (concentration of compound required for 50% inhibition of *SmpNP*) were determined (Table 3). As can be seen, compound **2**

was the most potent with an  $\text{IC}_{50}$  value of 86  $\mu\text{M}$ . This is a valuable result since thioxothiazolidinones as PNP inhibitors have not been described in the literature. In this context, it is particularly important for the *SmpNP* enzyme since the first class of inhibitors has recently been described in the literature.<sup>22</sup>

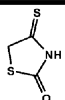
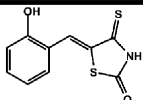
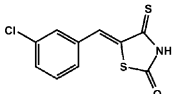
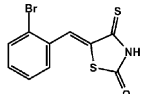
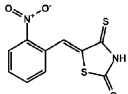
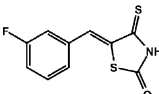
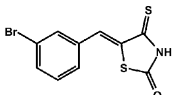
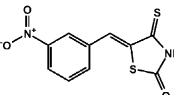
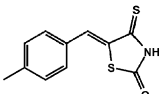
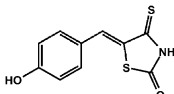
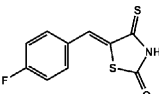
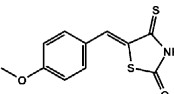
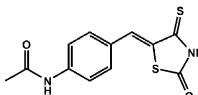
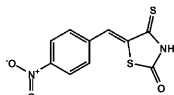
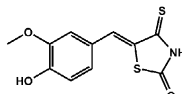
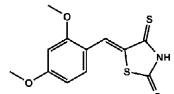
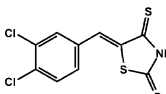
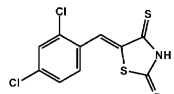
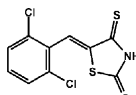
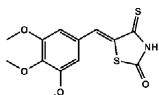
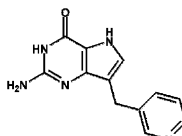
Based on these encouraging results, we have further explored this novel class of inhibitors employing the common thioxothiazolidinone core as a useful template for the synthesis of analogs. The design of the new analogs was based on our previous SAR and crystallographic studies with *SmpNP* inhibitors,<sup>22</sup> which indicated that potent 9-deaza-guanine derivatives exhibited bulky substituents at the nine position that favorably contribute to the enhancement of the biological activity. The crystallographic complex between *SmpNP* and BCX-34 (PDB ID 3DJF) revealed that its bulky substituent (*meta*-substituted pyridine) interacts to the side chains of Val262, Met221, and Tyr202 in the enzyme binding pocket (Figure 4C). Accordingly, these amino acid residues could be explored as potential sites to enhance potency and selectivity toward the parasite enzyme. In light of this, a variety of synthetically useful substituted phenyl groups was incorporated into the thioxothiazolidinone core to explore the SAR underlying this class of inhibitors. As can be seen in Table 3, we have prepared a series of 17 5-substituted-arylidene-4-thioxo-thiazolidin-2-ones (**4–20**), according to procedures described previously.<sup>37–40</sup>

In order to better understand and assess the molecular aspects involved in the inhibition of *SmpNP*, we have determined values of  $\text{IC}_{50}$  for the whole series of thioxothiazolidinones (**1–20**, Table 3). The results indicate that, in addition to compounds **2** and **3**, the compounds **4**, **7**, **10**, **11**, and **15–18** also showed substantial inhibition with  $\text{IC}_{50}$  values in the range of 12–198  $\mu\text{M}$ . For compounds **5**, **6**, **8**, **9**, **12–14**, and **20** (the weakest inhibitors of the series with  $\text{IC}_{50}\text{s} > 200 \mu\text{M}$ ),  $\text{IC}_{50}$  values could not be determined accurately due to solubility limitations that appeared to decrease the sensitivity of the assay. The *ortho*-, *meta*-, and *para*-nitrophenyl-substituted derivatives (**5**, **8**, and **14**, respectively) showed low inhibition of *SmpNP*, with  $\text{IC}_{50}\text{s} > 200 \mu\text{M}$ . The same occurred for the *meta*- and *para*-fluorophenyl-substituted derivatives (**6** and **11**, respectively), with  $\text{IC}_{50}$  values of 195  $\mu\text{M}$  and  $>200 \mu\text{M}$ , respectively. Other monosubstituted phenyl thioxothiazolidinone derivatives with a *para*-methyl (**9**), *para*-methoxy (**12**), and *para*-acetamide (**13**) also showed low inhibitory potential, with IC values  $>200 \mu\text{M}$ . In contrast, the *ortho*- and *meta*-bromophenyl- (**4** and **7**, respectively) and the *para*-hydroxyphenyl- (**10**) substituted derivatives showed significant inhibition of *SmpNP*, with  $\text{IC}_{50}$  values of 121, 12, and 18  $\mu\text{M}$ , respectively. The disubstituted phenyl thioxothiazolidinone derivatives 3-methoxy-4-hydroxy (**15**), 2,4-dimethoxy (**16**), 3,4-dichloro (**17**), 2,4-dichloro (**18**) and 2,6-dichloro (**19**) showed moderate to substantial inhibition, with  $\text{IC}_{50}$  values ranging from 38 to 191  $\mu\text{M}$ . The only trisubstituted phenyl derivative 3,4,5-trimethoxy (**20**) showed low inhibitory potency ( $\text{IC}_{50} > 200 \mu\text{M}$ ). The most potent inhibitors of the series **7**, **10**, and **17** ( $\text{IC}_{50} = 12, 18$ , and 38  $\mu\text{M}$ , respectively) were selected for further kinetic studies for determination of the mode of inhibitor interaction.

**Mechanism of Inhibition and Mode of Interaction.** The pharmacophore-based virtual screening approach employed



**Table 3.** Structures of the Thioxothiazolidinones **1–20** and Values of  $IC_{50}$  on *Sm*PNP

Compound	Structure	$IC_{50}$ ( $\mu$ M)	Compound	Structure	$IC_{50}$ ( $\mu$ M)
<b>1</b>		> 200	<b>2</b>		$86 \pm 7$
<b>3</b>		$198 \pm 15$	<b>4</b>		$121 \pm 10$
<b>5</b>		> 200	<b>6</b>		> 200
<b>7</b>		$12 \pm 1$	<b>8</b>		> 200
<b>9</b>		> 200	<b>10</b>		$18 \pm 2$
<b>11</b>		$195 \pm 18$	<b>12</b>		> 200
<b>13</b>		> 200	<b>14</b>		> 200
<b>15</b>		$72 \pm 6$	<b>16</b>		$191 \pm 17$
<b>17</b>		$38 \pm 2$	<b>18</b>		$74 \pm 6$
<b>19</b>		$70 \pm 6$	<b>20</b>		> 200
<b>21*</b>		$0.8 \pm 0.07$			

\* Compound **21**, a known *Sm*PNP inhibitor,<sup>22</sup> was used as a positive control for enzyme inhibition.

in this study was designed to identify potential *Sm*PNP inhibitors that could bind directly to the free form of the enzyme at the substrate binding site. In this case, one would expect that the identified lead candidates **7**, **10**, and **17** interact with the target enzyme through a competitive reversible binding mechanism. To explore the mechanism of inhibition in more detail, we have determined the  $K_i$  values and the type of inhibition with respect to the physiological substrate inosine, employing compounds **7**, **10**, and **17** (Figure 6A–C). Because the mode of inhibitor type defines the binding relationships between the free enzyme (E), substrate (S) and enzyme–substrate (E·S) species to the inhibitor (I), this study allowed the development of mechanism-based SARs, which are highly desirable for the rational design of enzyme inhibitors. The results shown in Figure 6 indicate that the inhibition of *Sm*PNP was found to be

competitive with respect to inosine. The Lineweaver–Burk double-reciprocal plots show intercepts of all lines (obtained at three different inhibitor concentrations) converging at the y-axis ( $1/V_{\max}$ ), whereas the slope ( $K_M/V_{\max}$ ) and the x-axis intercepts ( $-1/K_M$ ) vary with inhibitor concentration. Consequently, the  $V_{\max}$  values remain constant, whereas the apparent values of  $K_M$  ( $K_M^{\text{app}}$ , defined as  $K_M(1 + [I]/K_i)$ ) increase with increasing inhibitor concentrations. This behavior is consistent with a mutually exclusive binding mode between inhibitor and substrate, therefore, these inhibitors (**7**, **10**, and **17**) compete with inosine for the free enzyme active site.<sup>41</sup> Another factor that must be considered in inhibitor drug design is the comparisons on the rational basis of the enzyme dissociation constant ( $K_i$ ), since  $IC_{50}$  values can vary with substrate concentration for competitive inhibitors. The same data of Figure 6 was employed to determine

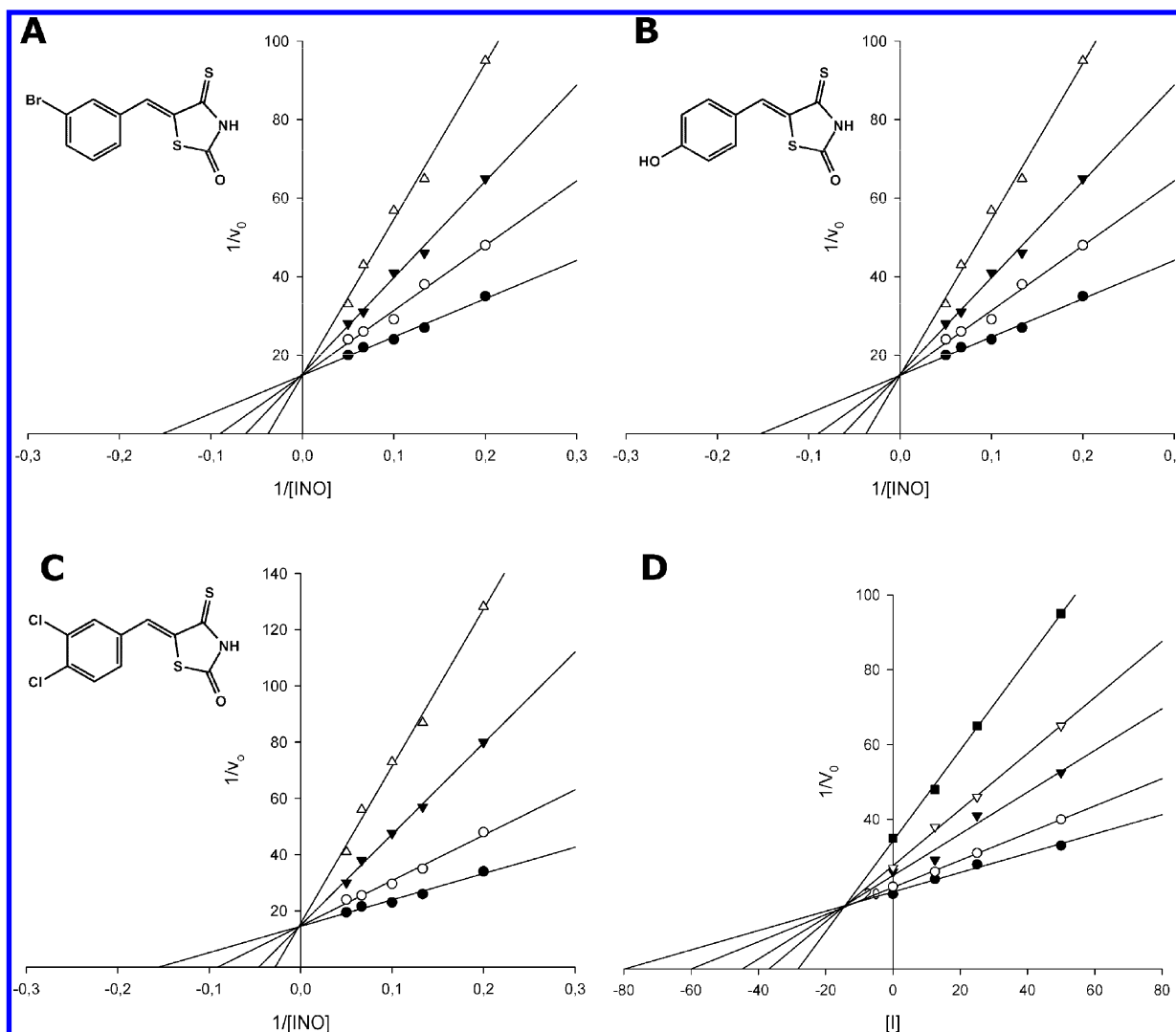


**Figure 6.** Competitive inhibitory profile of *SmPNP* inhibitors: (A) **7** ( $K_i = 9 \mu\text{M}$ ), (B) **10** ( $K_i = 12 \mu\text{M}$ ), and (C) **17** ( $K_i = 18 \mu\text{M}$ ). Kinetic activity was assayed in the presence of increasing concentrations of inhibitors. (A) 20 (○), 40 (▼), and 80  $\mu\text{M}$  (Δ) and absence of inhibitor (●). (B) 12.5 (○), 25 (▼), and 50  $\mu\text{M}$  (Δ) and absence of inhibitor (●). (C) 7 (○), 20 (▼), and 40 (Δ) and absence of inhibitor (●). (D) Representative Dixon plot of the competitive inhibitor **10**. The concentration of inosine employed in each case was 5 (■), 7.5 (Δ), 10 (▼), 15 (○), and 20  $\mu\text{M}$  (●). The concentration of inhibitor varied between 12.5 and 50  $\mu\text{M}$ .

$K_i$  values of the competitive inhibitors using Dixon plots, which consists of plotting the reciprocal of the initial velocity ( $1/v_0$ ) versus a series of inhibitor concentrations at constant substrate concentration, where the lines converge above the  $x$ -axis, indicating the inhibition constant  $-K_i$  (Figure 6D).  $K_i$  values of 9, 12, and 18  $\mu\text{M}$  were obtained for the *SmPNP* inhibitors **7**, **10**, and **17**, respectively. Accordingly, these results confirm the successful use of our structure-based virtual screening strategy, allowing the discovery of these thioxothiazolidinone derivatives as a new class of competitive inhibitors of *SmPNP*, with affinity values in the low-micromolar range.

On the basis of the information collected in the course of this work, molecular modeling studies were carried out in order to further understand the mode of interaction of these inhibitors. To achieve this, the most potent inhibitor **7** was docked into the active site of *SmPNP*. Although a quantitative agreement between model and experimental SAR data was not expected, the model provided relevant insights into the inhibitory activity of the thioxothiazolidinone derivatives. The best pose of **7** within the *SmPNP* binding pocket is shown in Figure 7. The *meta*-bromophenyl substituent is

oriented toward the hydrophobic side chain of Ala118, Val262, His259, Met221, and Phe161, partially satisfying the pharmacophore requirements. The phenyl ring undergoes  $\pi$ -stacking with the side chain of Phe161 in a classic T-shaped arrangement, whereas the bromine atom is in van der Waals contact with the side chain of Ala 118 and Val262. These findings are in agreement with our SAR data, which indicates that the presence of bulky and neutral groups at the *meta*-position of phenyl ring attached to the thioxothiazolidinone core structure is favorable for enhanced inhibitory activity. In addition, this conformation also suggests a structural feature that might be involved in the preferential binding of the *para*-hydroxylphenyl substituent of **10** to *SmPNP* in comparison with the corresponding *para*-methyl (**9**), *para*-fluorine (**11**), *para*-acetamide (**13**), and *para*-nitro (**14**) substituents. According to the model, the His259 residue would be a possible hydrogen-bonding site to interact with complementary sites of the inhibitor in order to incorporate selected molecules inside the binding cavity of the enzyme, thereby contributing to the improved potency of the inhibitor **10**. On the other hand, the low potency observed for the

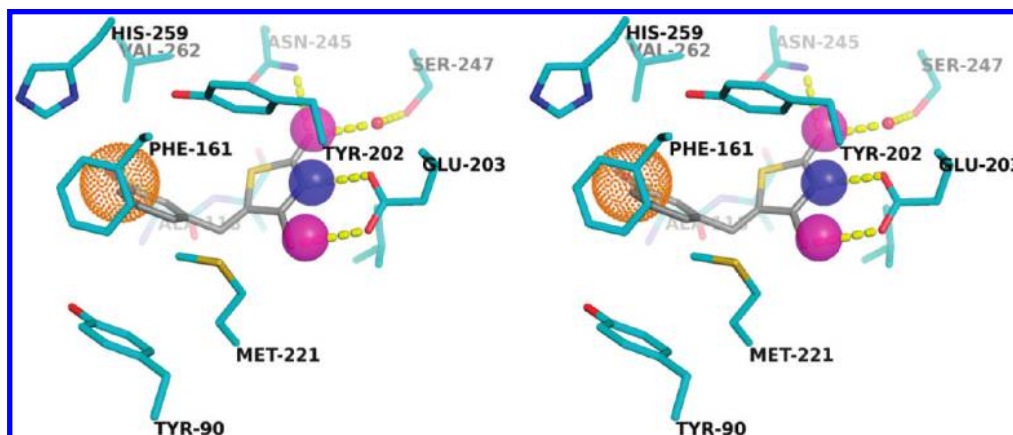


**Figure 7.** Stereo view of the best-docked pose of compound **17** (gray) within the *Sm*PNP binding pocket (cyan). The target-based pharmacophore features are described in Figure 4, and hydrogen bonds are depicted as yellow dashed lines.

*meta*-phenyl substituted analogs might be due to steric hindrance to the side chain of Met221 and the main chain of Ala118.

## CONCLUSION

The development of new antiparasitic agents is one of the most important challenges of the 21st century.<sup>8,9,22</sup> In this work, we described the development and validation of a 3D pharmacophore-based virtual screening approach for *S. mansoni* purine nucleoside phosphorylase (*Sm*PNP) inhibitors, leading to the identification of three small-molecule thioxothiazolidinones (**1–3**) with in vitro inhibitory activity. Subsequent structure–activity relationship (SAR) studies yielded a new series of competitive inhibitors with IC<sub>50</sub> values in the low-micromolar level. Compounds **7**, **10**, and **17** are promising lead candidates for future medicinal chemistry efforts designed to discover competitive inhibitors of *Sm*PNP having increased potency.

## MATERIAL AND METHODS

**Computational Approach.** The pharmacophore search and docking calculations were performed using the SYBYL 8.0 package (Tripos Inc., St. Louis, MO) running on Red Hat Enterprise Linux workstations. The 3D structures of the inhibitors were generated using standard geometric parameters of the molecular modeling software package SYBYL 8.0. Each single optimized conformation of each molecule in the data set was energetically minimized employing the Tripos force field<sup>42</sup> and the Powell conjugate gradient algorithm<sup>43</sup> with a convergence criterion of 0.05 kcal/mol·Å. Partial atomic charges were calculated by the Gasteiger–Hückel method.<sup>44</sup> The analyses, calculations, and visualizations were performed using the programs SYBYL 8.0 and Pymol (DeLano Scientific, Palo Alto, CA).<sup>45</sup>

**Pharmacophore Model.** The crystal structures of *Sm*PNP (PDB IDs 1TCU, 1TCV, 1TD1, 3DJF, 3FNQ, 3FAZ, 3FB1, 3E9R, 3F8W, 3IEX, 3E9Z, and 3E0Q) and *Bt*PNP (PDB IDs 1A9O, 1A9P, 1A9Q, 1A9R, 1A9S, 1A9T, 1FXU, 1V48, 2QPL, 3PNP, and 4PNP) in complex with several ligands were superimposed by least-squares fit of the C $\alpha$  atoms. The pharmacophore model was generated taking into account important molecular and physicochemical characteristics of the binding site. This resulted in a four-point pharmacophore of deviating spherical tolerances (Figure 4C), each assigned

to a specific property. Three spheres were used to define the position and orientation of the putative donor and acceptor sites. The first pharmacophore point was assigned as a donor/acceptor site close to Asn245 and the crystallographic water molecule; the second (donor site) and third (donor/acceptor site) pharmacophore points were determined close to Glu203; as long as the fourth point was derived to describe the favorable region for hydrophobic interactions adjacent to the residues Met221 and Val262.

**3D Database Pharmacophore Searching.** The structures of 851 385 compounds from three commercially available chemical libraries (ChemBridge, Asinex, and Ambinter) were obtained from the ZINC database.<sup>30</sup> First, only the molecules containing H, C, N, O, S, P, F, Cl, Br, or I were selected. Second, the fraction of compounds consistent with the widely used Lipinski's "rule of 5",<sup>31</sup> molecular weight (MW)  $\leq$  500 Da; cLog *P*  $\leq$  5; hydrogen-bond donors (OH and NH)  $\leq$  5; hydrogen-bond acceptors (O or N)  $\leq$  10 was reduced to 300 563 compounds, whose 3D structures were then transferred into the UNITY databases in SYBYL 8.0. The 3D search with UNITY was based on the generated pharmacophore model. Thus, in order to employ the pharmacophore model as 3D constraints, the crystallographic spatial coordinates of the ligand 2-amino-7-(pyridin-3-ylmethyl)-3,5-dihydro-4H-pyrrolo[3,2-d]pyrimidin-4-one (BCX-34) bound to *Sm*PNP (PDB ID 3DJF) were used. The donor and acceptor features were defined by connecting the donor and the acceptor atoms of the ligand via the partial match utility. To consider the directionality of the hydrogen bonds, the corresponding sites were attributed to the neighboring atoms of the protein and the crystallographic water molecule. The hydrophobic feature was partially characterized as the centroid of the pyridinyl ring of BCX-34. The diameters of the spheres were adjusted in such a way that the test sample composed of known PNP ligands (Table 1) could be retrieved.

**Molecular Modeling.** The X-ray crystallographic data for *Sm*PNP in complex with BCX-34 used in docking simulations were retrieved from PDB (PDB ID 3DJF). For the calculations, hydrogen atoms were added in standard geometry, including the catalytic Glu203, using the Biopolymer module as implemented in SYBYL 8.0. The histidine, glutamine, and asparagine residues in the active binding site were manually checked for possible flipped orientation, protonation, and tautomeric states with a Pymol 0.99 side-

chain wizard script. The active site was defined incorporating all amino acid residues within a radius sphere of 6.0 Å centered on the bound ligand, including the crystallographic water molecule, which was considered part of the binding site during the docking simulations. Molecular modeling studies were carried out using the default parameters of FlexX (BioSolveIT, Sankt Augustin, Germany). The FlexX scoring function was employed to select the representative pose for each compound. These solutions were visually checked to find the best score that matches the original pharmacophore hypothesis. The visual inspection is a common practice which is important to avoid testing false positives due to assumptions and shortcomings in docking methods and scoring functions.<sup>46</sup> In the visual inspection we critically assessed the suggested binding conformation, the mutual surface complementarity of ligand and protein, and the possible presence of unfilled space along the protein–ligand interface. In light of this, it was judged important that there was a complementarity of the ligand and protein surfaces, reasonable internal geometry of the ligand in the binding pose, proximity of the hydrophobic substituent of the ligand to the protein cavity formed by Met221 and Val262 residues, and that reasonable hydrogen-bonding interactions, typically with the separation of donor and acceptor groups in the range 2.4–3.5 Å. Subsequently, the top-ranked conformations for each compound were submitted to the Web-based interface DrugScore<sup>ONLINE</sup> to rescore the proposed binding mode.<sup>34,47</sup> Finally, the individual ranks obtained from the consensus scoring were considered to establish a new rank order list where the top-ranked ligands with innovative scaffolds were selected for biological evaluation.

**Chemistry and Kinetic Measurements.** *SmpNP* was expressed and purified as described previously.<sup>23,28</sup> Xanthine oxidase was of the best grade available from Sigma Aldrich and was used without further purification. The compounds **1–3** and all other reagents and solvents were obtained commercially from either Sigma Aldrich or Ambinter and were of the highest purity available. The compounds **4–20** were synthesized and characterized according to procedures described previously.<sup>37–40</sup> The purity of the compounds was equal to or greater than 95% as verified by high-performance liquid chromatography. Kinetic measurements were carried out spectrophotometrically with the aid of a Cary100 UV–vis spectrophotometer, using a standard coupled assay as previously described.<sup>19,22,35,36</sup> The reaction mixture contained 5 nM *SmpNP* (as the monomer), 50 mM fosfate buffer (KPO<sub>4</sub>, pH 7.4), 10 μM inosine, and xanthine oxidase 40 milliunits/mL. Uric acid formation was monitored at 293 nm, in triplicate at 25 °C (extinction coefficient for uric acid,  $\epsilon_{293} = 12.9 \text{ mM}^{-1}$ ).<sup>48</sup> The percentage of inhibition was calculated according to the following equation:

$$\% \text{inhibition} = 100 \times (1 - V_i/V_0)$$

where,  $V_i$  and  $V_0$  are the initial velocities (enzyme activities) determined in the presence and absence of inhibitor, respectively. Compound **21**, a known *SmpNP* inhibitor, was used as a positive control for enzyme inhibition.<sup>22</sup> Values of  $\text{IC}_{50}$  were independently determined by making rate measurements for at least six inhibitor concentrations. The type of inhibition and  $K_i$  values were determined under the same experimental

conditions for three different inhibitor concentrations at five varying substrate concentrations (5.0, 7.5, 10, 15, and 20 μM). All kinetic parameters were determined from the collected data by nonlinear regression employing the SigmaPlot enzyme kinetics module. The values represent means of at least three individual experiments.

## ACKNOWLEDGMENT

We gratefully acknowledge financial support from FAPESP (The State of Sao Paulo Research Foundation) and CNPq (The National Council for Scientific and Technological Development), Brazil.

## REFERENCES AND NOTES

- (1) Steinmann, P.; Keiser, J.; Bos, R.; Tanner, M.; Utzinger, J. Schistosomiasis and Water Resources Development: Systematic Review, Meta-Analysis, and Estimates of People at Risk. *Lancet Infect. Dis.* **2006**, *6*, 411–425.
- (2) Fenwick, A.; Webster, J. P.; Bosque-Oliva, E.; Blair, L.; Fleming, F. M.; Zhang, Y.; Garba, A.; Stothard, J. R.; Gabrielli, A. F.; Clements, A. C.; Kabatereine, N. B.; Toure, S.; Demebele, R.; Nyandindi, U.; Mwansa, J.; Koukounari, A. The Schistosomiasis Control Initiative (SCI): Rationale, Development and Implementation from 2002–2008. *Parasitology* **2009**, *136*, 1719–1730.
- (3) Hagan, P.; Appleton, C. C.; Coles, G. C.; Kusel, J. R.; Tchuente, L. A. Schistosomiasis Control: Keep Taking the Tablets. *Trends Parasitol.* **2004**, *20*, 92–97.
- (4) Fenwick, A.; Savioli, L.; Engels, D.; Robert Bergquist, N.; Todd, M. H. Drugs for the Control of Parasitic Diseases: Current Status and Development in Schistosomiasis. *Trends Parasitol.* **2003**, *19*, 509–515.
- (5) Hotez, P. J.; Molyneux, D. H.; Fenwick, A.; Kumaresan, J.; Sachs, S. E.; Sachs, J. D.; Savioli, L. Control of Neglected Tropical Diseases. *N. Engl. J. Med.* **2007**, *357*, 1018–1027.
- (6) Sabra, A. N.; Botros, S. S. Response of *Schistosoma mansoni* Isolates Having Different Drug Sensitivity to Praziquantel Over Several Life Cycle Passages With and Without Therapeutic Pressure. *J. Parasitol.* **2008**, *94*, 537–541.
- (7) Guido, R. V. C.; Oliva, G.; Andricopulo, A. D. Virtual Screening and Its Integration With Modern Drug Design Technologies. *Curr. Med. Chem.* **2008**, *15*, 37–46.
- (8) Andricopulo, A. D.; Salum, L. B.; Abraham, D. J. Structure-Based Drug Design Strategies in Medicinal Chemistry. *Curr. Top. Med. Chem.* **2009**, *9*, 771–790.
- (9) Guido, R. V. C.; Oliva, G. Structure-Based Drug Design for Tropical Diseases. *Curr. Top. Med. Chem.* **2009**, *9*, 824–843.
- (10) Guido, R. V. C.; Balliano, T. L.; Andricopulo, A. D.; Oliva, G. Kinetic and Crystallographic Studies on Glyceraldehyde-3-Phosphate Dehydrogenase from *Trypanosoma cruzi* in Complex With Iodoacetate. *Lett. Drug Des. Discovery* **2009**, *6*, 210–214.
- (11) Guido, R. V. C.; Castilho, M. S.; Mota, S. G. R.; Oliva, G.; Andricopulo, A. D. Classical and Hologram QSAR Studies on a Series of Inhibitors of Trypanosomatid Glyceraldehyde-3-Phosphate Dehydrogenase. *QSAR Comb. Sci.* **2008**, *27*, 768–781.
- (12) Guido, R. V. C.; Oliva, G.; Montanari, C. A.; Andricopulo, A. D. Structural Basis for Selective Inhibition of Trypanosomatid Glyceraldehyde-3-Phosphate Dehydrogenase: Molecular Docking and 3D QSAR Studies. *J. Chem. Inf. Model.* **2008**, *48*, 918–929.
- (13) Guido, R. V. C.; Trossini, G. H.; Castilho, M. S.; Oliva, G.; Ferreira, E. I.; Andricopulo, A. D. Structure-Activity Relationships for a Class of Selective Inhibitors of the Major Cysteine Protease from *Trypanosoma cruzi*. *J. Enzyme Inhib. Med. Chem.* **2008**, *23*, 964–973.
- (14) Trossini, G. H.; Guido, R. V. C.; Oliva, G.; Ferreira, E. I.; Andricopulo, A. D. Quantitative Structure Activity Relationships for a Series of Inhibitors of Cruzain from *Trypanosoma cruzi*: Molecular Modeling, CoMFA and CoMSIA Studies. *J. Mol. Graph. Modell.* **2009**, *28*, 3–11.
- (15) Cavazzuti, A.; Paglietti, G.; Hunter, W. N.; Gamarro, F.; Piras, S.; Loriga, M.; Allecca, S.; Corona, P.; McLuskey, K.; Tulloch, L.; Gibellini, F.; Ferrari, S.; Costi, M. P. Discovery of Potent Pteridine Reductase Inhibitors to Guide Antiparasite Drug Development. *Proc. Nat. Acad. Sci. U.S.A.* **2008**, *105*, 1448–1453.
- (16) Brak, K.; Doyle, P. S.; McKerrow, J. H.; Ellman, J. A. Identification of a New Class of Nonpeptidic Inhibitors of Cruzain. *J. Am. Chem. Soc.* **2008**, *130*, 6404–6410.



- (17) Nowicki, M. W.; Tulloch, L. B.; Worrall, L.; McNae, I. W.; Hannaert, V.; Michels, P. A.; Fothergill-Gilmore, L. A.; Walkinshaw, M. D.; Turner, N. J. Design, Synthesis and Trypanocidal Activity of Lead Compounds Based on Inhibitors of Parasite Glycolysis. *Bioorg. Med. Chem.* **2008**, *16*, 5050–5061.
- (18) Kohring, K.; Wiesner, J.; Altenkamper, M.; Sakowski, J.; Silber, K.; Hillebrecht, A.; Haebel, P.; Dahse, H. M.; Ortmann, R.; Jomaa, H.; Klebe, G.; Schlitzer, M. Development of Benzophenone-Based Farnesyltransferase Inhibitors as Novel Antimalarials. *ChemMedChem* **2008**, *3*, 1217–1231.
- (19) Castilho, M. S.; Postigo, M. P.; de Paula, C. B.; Montanari, C. A.; Oliva, G.; Andricopulo, A. D. Two- and Three-Dimensional Quantitative Structure-Activity Relationships for a Series of Purine Nucleoside Phosphorylase Inhibitors. *Bioorg. Med. Chem.* **2006**, *14*, 516–527.
- (20) Clinch, K.; Evans, G. B.; Frohlich, R. F.; Furneaux, R. H.; Kelly, P. M.; Legentil, L.; Murkin, A. S.; Li, L.; Schramm, V. L.; Tyler, P. C.; Woolhouse, A. D. Third-Generation Immucillins: Syntheses and Bioactivities of Acyclic Immucillin Inhibitors of Human Purine Nucleoside Phosphorylase. *J. Med. Chem.* **2009**, *52*, 1126–1143.
- (21) Mason, J. M.; Murkin, A. S.; Li, L.; Schramm, V. L.; Gainsford, G. J.; Skelton, B. W. A Beta-Fluoroamine Inhibitor of Purine Nucleoside Phosphorylase. *J. Med. Chem.* **2008**, *51*, 5880–5884.
- (22) Castilho, M. S.; Postigo, M. P.; Pereira, H. M.; Oliva, G.; Andricopulo, A. D. Structural basis for selective inhibition of purine nucleoside phosphorylase from *Schistosoma mansoni*: Kinetic and structural studies. *Bioorg. Med. Chem.* **2010**, *18*, 1421–1427.
- (23) Pereira, H. M.; Rezende, M. M.; Castilho, M. S.; Oliva, G.; Garratt, R. C. Adenosine binding to low-molecular-weight purine nucleoside phosphorylase: the structural basis for recognition based on its complex with the enzyme from *Schistosoma mansoni*. *Acta Crystallogr., Sect. D: Biol. Crystallogr.* **2010**, *D66*, 73–79.
- (24) Pereira, H. M.; Franco, G. R.; Cleasby, A.; Garratt, R. C. Structures for the potential drug target purine nucleoside phosphorylase from *schistosoma mansoni* causal agent of schistosomiasis. *J. Mol. Biol.* **2005**, *353*, 584–599.
- (25) Mao, C.; Cook, W. J.; Zhou, M.; Federov, A. A.; Almo, S. C.; Ealick, S. E. Calf Spleen Purine Nucleoside Phosphorylase Complexed With Substrates and Substrate Analogues. *Biochemistry* **1998**, *37*, 7135–7146.
- (26) Luic, M.; Koellner, G.; Shugar, D.; Saenger, W.; Bzowska, A. Calf Spleen Purine Nucleoside Phosphorylase: Structure of Its Ternary Complex With an N(7)-Acycloguanosine Inhibitor and a Phosphate Anion. *Acta Crystallogr., Sect. D: Biol. Crystallogr.* **2001**, *57*, 30–36.
- (27) Luic, M.; Koellner, G.; Yokomatsu, T.; Shibuya, S.; Bzowska, A. Calf Spleen Purine-Nucleoside Phosphorylase: Crystal Structure of the Binary Complex With a Potent Multisubstrate Analogue Inhibitor. *Acta Crystallogr., Sect. D: Biol. Crystallogr.* **2004**, *60*, 1417–1424.
- (28) Pereira, H. M.; Berdini, V.; Cleasby, A.; Garratt, R. C. Crystal structure of Calf Spleen Purine Nucleoside Phosphorylase Complexed to a Novel Purine Analogue. *FEBS Lett.* **2007**, *581*, 5082–5086.
- (29) Guido, R. V. C.; Castilho, M. S.; Oliva, G.; Andricopulo, A. D. Structure-Based Pharmacophore Strategies in Drug Design. In *Current Methods in Medicinal Chemistry and Biological Physics*. 1st ed.; Taft, C. A. Silva, C. H. T. P., Eds.; Research Signpost: Kerala, India, 2008; Vol. 2, pp 1–19.
- (30) Wermuth, C. G.; Ganellin, C. R.; Lindberg, P.; Mitscher, L. A. Glossary of Terms Used in Medicinal Chemistry (IUPAC Recommendations 1998). *Pure Appl. Chem.* **1998**, *70*, 1129–1143.
- (31) Irwin, J. J.; Shoichet, B. K. ZINC - A Free Database of Commercially Available Compounds for Virtual Screening. *J. Chem. Inf. Model.* **2005**, *45*, 177–182.
- (32) Lipinski, C. A.; Lombardo, F.; Dominy, B. W.; Feeney, P. J. Experimental and Computational Approaches to Estimate Solubility and Permeability in Drug Discovery and Development Settings. *Adv. Drug Delivery Rev.* **2001**, *46*, 3–26.
- (33) *UNITY Chemical Information Software*, version 4.1; Tripos Inc.: St. Louis, MO, 2006.
- (34) Rarey, M.; Kramer, B.; Lengauer, T.; Klebe, G. A Fast Flexible Docking Method Using an Incremental Construction Algorithm. *J. Mol. Biol.* **1996**, *261*, 470–489.
- (35) Gohlke, H.; Hendlich, M.; Klebe, G. Knowledge-Based Scoring Function to Predict Protein-Ligand Interactions. *J. Mol. Biol.* **2000**, *295*, 337–356.
- (36) Andricopulo, A. D.; Yunes, R. A. Structure-Activity Relationships for a Collection of Structurally Diverse Inhibitors of Purine Nucleoside Phosphorylase. *Chem. Pharm. Bull.* **2001**, *49*, 10–17.
- (37) Farutin, V.; Masterson, L.; Andricopulo, A. D.; Cheng, J.; Riley, B.; Hakimi, R.; Frazer, J. W.; Cordes, E. H. Structure-Activity Relationships for a Class of Inhibitors of Purine Nucleoside Phosphorylase. *J. Med. Chem.* **1999**, *42*, 2422–2431.
- (38) Gouveia, F. L.; de Oliveira, R. M.; de Oliveira, T. B.; da Silva, I. M.; do Nascimento, S. C.; de Sena, K. X.; de Albuquerque, J. F. Synthesis, Antimicrobial and Cytotoxic Activities of Some 5-Arylidene-4-Thioxo-Thiazolidine-2-Ones. *Eur. J. Med. Chem.* **2009**, *44*, 2038–2043.
- (39) Albuquerque, J. F.; Andrade, A. M.; Barros, A. L.; Nascimento, M. R.; Ximenes, E. A.; Galdino, S. L.; Pitta, I. R.; Perrissin, M. Substituted Thiazolidinediones and Thioxothiazolidinones: Synthesis and Structure. *Ann. Pharm. Fr.* **1999**, *57*, 385–391.
- (40) Albuquerque, J. F.; Azevedo, L. C.; Galdino, S. L.; Chantegrel, J.; Pitta, I. R.; Luu-Duc, C. Synthesis and Structural Study of 5-arylidene thiazolidine-2,4-diones and 3-Substituted-4-Thio-Imidazolidine-2-Ones. *Ann. Pharm. Fr.* **1995**, *53*, 209–214.
- (41) Chantegrel, J.; Albuquerque, J. C.; Guarda, V. L.; Perrissin, M.; Lima, M. C.; Galdino, S. L.; Brandao, S. S.; Thomasson, F.; Pitta, I. R.; Luu-Duc, C. New Substituted 4-Thioxothiazolidine-2-One Derivatives: Synthesis and Structural Study. *Ann. Pharm. Fr.* **2002**, *60*, 403–409.
- (42) Copeland, R. A. Reversible Modes of Inhibitor Interactions with Enzymes. In *Evaluation of Enzyme Inhibitors in Drug Discovery: a guide for medicinal chemists and pharmacologists. Methods of Biochemical Analysis*. Wiley-Interscience: Hoboken, NJ, 2005; Vol. 46, pp 48–81.
- (43) Clark, M.; Cramer, R. D.; Van Opdenbosch, N. Validation of the General Purpose Tripos 5.2 Force Field. *J. Comput. Chem.* **1989**, *10*, 982–1012.
- (44) Powell, M. J. D. Restart Procedures for the Conjugate Gradient Method. *Math. Program.* **1977**, *12*, 241–254.
- (45) Gasteiger, J.; Marsili, M. Iterative Partial Equalization of Orbital Electronegativity - A Rapid Access to Atomic Charges. *Tetrahedron* **1980**, *36*, 3219–3228.
- (46) Klebe, G. Virtual screening: Scope and limitation. In *Virtual Screening in Drug Discovery*, 1st ed.; Alvarez, J., Shoichet, B., Eds.; CRC Press: Boca Raton, FL, 2005, Vol. 1, pp 3–24.
- (47) DrugScore<sup>ONLINE</sup>, V0.9 - Scoring Functions for Protein-Ligand Complexes; Institut für Pharmazeutische Chemie: Marburg, Germany; <http://www.agklebe.de>. Accessed on November 17, 2009.
- (48) Kim, B. K.; Cha, S.; Parks, R. E., Jr. Purine Nucleoside Phosphorylase from Human Erythrocytes. II. Kinetic Analysis and Substrate-Binding Studies. *J. Biol. Chem.* **1968**, *243*, 1771–1776.

CI100128K